

Towards a direct transition energy measurement of the lowest nuclear excitation in ^{229}Th

L. v.d. Wense^{a,b}, P.G. Thirolf^{a*}, D. Kalb^a and M. Laatiaoui^{c,d}

^aLudwig-Maximilians-Universität München, Am Coulombwall 1, Garching, Germany

^bMax-Planck-Institute f. Quantenoptik, Hans-Kopfermann-Str. 1, Garching, Germany,

^cGSI Helmholtzzentrum für Schwerionenforschung GmbH, Planckstr. 1, Darmstadt, Germany,

^dHelmholtz Institut Mainz, Johann-Joachim-Becherweg 36, Germany

E-mail: Peter.Thirolf@physik.uni-muenchen.de

ABSTRACT: The isomeric first excited state of the isotope ^{229}Th exhibits the lowest nuclear excitation energy in the whole landscape of known atomic nuclei. For a long time this energy was reported in the literature as 3.5(5) eV, however, a new experiment corrected this energy to 7.6(5) eV, corresponding to a UV transition wavelength of 163(11) nm. The expected isomeric lifetime is $\tau = 3\text{-}5$ hours, leading to an extremely sharp relative linewidth of $\Delta E/E \approx 10^{-20}$, 5-6 orders of magnitude smaller than typical atomic relative linewidths. For an adequately chosen electronic state the frequency of the nuclear ground-state transition will be independent from influences of external fields in the framework of the linear Zeeman and quadratic Stark effect, rendering ^{229m}Th a candidate for a reference of an optical clock with very high accuracy [1]. Moreover, in the literature speculations about a potentially enhanced sensitivity of the ground-state transition of ^{229m}Th for eventual time-dependent variations of fundamental constants (e.g. fine structure constant α) can be found [2, 3].

We report on our experimental activities that aim at a direct identification of the UV fluorescence of the ground-state transition energy of ^{229m}Th . A further goal is to improve the accuracy of the ground-state transition energy as a prerequisite for a laser-based optical control of this nuclear excited state, allowing to build a bridge between atomic and nuclear physics and open new perspectives for metrological as well as fundamental studies.

KEYWORDS: ^{229m}Th , nuclear clock, UV fluorescence.

*Corresponding author.

Contents

| | |
|---|-----------|
| 1. Introduction | 2 |
| 2. Experimental approach | 4 |
| 2.1 Stopping and extraction via a buffer-gas cell | 5 |
| 2.1.1 Population and Extraction of ^{229m}Th using the gas cell | 6 |
| 2.2 RF mass filter for exclusive extraction of ^{229}Th α recoil nuclei | 8 |
| 2.3 Setup of ion collection system | 10 |
| 2.4 Provisions against quenching processes | 11 |
| 2.5 Optimizing the UV focusing optics | 11 |
| 2.6 Detection of the ^{229m}Th UV fluorescence radiation | 14 |
| 2.7 Improved determination of ^{229m}Th ground-state transition | 14 |
| 3. Concluding efficiency assessment and count rate estimate | 15 |

1. Introduction

Amongst the presently about 2800 known isotopes, ^{229}Th occupies a special position due to its first excited state which exhibits the lowest excitation energy that so far has been identified in any of the known atomic nuclei (the next comparably low excitation energy can be found in ^{235}U with 73 eV). Since more than 30 years experiments have been performed to measure the energy splitting of the ground-state doublet in ^{229}Th (with spin and parity $J^\pi = 5/2^+, 3/2^+$, respectively and Nilsson quantum numbers [633] for the ground state and [631] for the first excited state) [4, 5, 6], without so far achieving a direct observation of the γ decay. The so far available data all originate from an analysis of combinations between higher-lying states that decay into the ground and first excited state, respectively.

For a long time 3.5 eV was generally adopted as value of the transition energy (in Ref. [6] quoted as (3.5 ± 1.0) eV), until an improved experiment of the Livermore group using a novel X-ray spectrometer resulted in a new and significantly altered value of 7.6(5) eV [7], recently updated to 7.8(5) eV [8]. This new value places the isomeric ^{229}Th ground-state transition in the spectral region of the deep UV (VUV: Vacuum UV), while the previous experiments had concentrated on the visual range of the electromagnetic spectrum. So far no unambiguous direct identification of this transition has been achieved. In contrast to the ground state of ^{229}Th with a half life of 7880 years, the

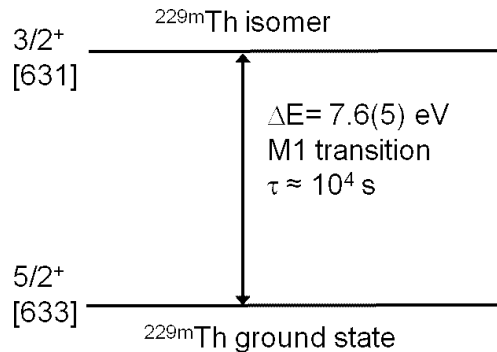


Figure 1. Almost degenerate ground-state doublet in ^{229}Th with the energetically lowest nuclear ground state and the isomeric first excited state at 7.6(5) eV.

first excited state represents a long-lived isomeric state with an (expected) half-life of some (2-4) hours. In view of the extremely low excitation energy and the long lifetime of the ^{229m}Th isomer, its unique properties are obvious: a natural linewidth of ca. $10 \mu\text{Hz}$ corresponds to an extremely sharp ground-state transition with $\Delta E/E \approx 10^{-20}$.

In general, nuclear transitions profit from the about 5 orders of magnitude smaller nuclear radii compared to the extension of atomic systems, leading to a much improved shielding against external perturbing fields and resulting in small nuclear multipole moments. Hereby the nuclear transition frequency is independent of all influences that lead to level shifts solely depending on electronic quantum numbers, since those do not change during the nuclear transition and therefore will be equally affected in both participating nuclear states. This holds for the scalar part of the quadratic Stark effect as the typically dominant reason of shifts of electronic transition frequencies under the influence of static electrical fields or electromagnetic radiation. The remaining influence of the so-called hyperfine Stark-drift can be estimated in the optical frequency range according

to [9] to a relative magnitude of 10^{-19} under the influence of the black-body radiation at room temperature. In order to avoid the influence of an external magnetic field via the linear Zeeman effect, an electronic state has to be chosen for the laser cooling and frequency detection, where the total angular momentum F of the atoms is an integer number. In this case the Zeeman component $m_F = 0 \rightarrow 0$ can be used, which shows only a weak contribution of the quadratic Zeeman effect at low magnetic fields, typically ranging below 1 kHz at 0.1 mT. If we can assume an efficient shielding of external magnetic fields (e.g. by multiple layers of μ metal) to below 1 nT, the remaining influence of external magnetic fields in ^{229}Th can be estimated to a relative contribution of only 10^{-18} .

Thus ^{229m}Th proves to be extraordinary insensitive to external perturbing effects in first order for magnetic fields and in second order for electric fields. This qualifies the isomeric nuclear transition in ^{229}Th , where the frequency is predominantly determined by the strong interaction, as a candidate for a frequency standard, extremely insensitive against frequency shifts. Therefore, a system could be realized that is complementary to present atomic frequency standards, which are based either completely or partly on the electromagnetic interaction with contributions by the strong force.

Additionally, a comparison of the temporal behaviour of the transition frequency of ^{229}Th with these established frequency standards could enable a new opportunity for a lab-based search for temporal variations of the coupling constants of the electromagnetic and strong interactions, as it is predicted in some Grand Unified Theories. This aspect has been extensively discussed in the literature in recent years, including speculations on potential enhancement mechanisms for the sensitivity to such temporal variations in the case of ^{229}Th [2, 3, 10, 11, 12].

In view of the intriguing potential of the outlined unique properties, already in the past numerous, however unsuccessful, attempts have been conducted to directly identify the first excited state of ^{229}Th . An obvious reason for this failure follows from the result of a spectroscopic measurement performed by the Livermore group [7], which resulted in a more than a factor of 2 modified value of the ground-state transition energy in ^{229m}Th of 7.6(5) eV, corresponding to a wavelength of 163(11) nm. Therefore this transition falls into the region of deep UV, where it could not be detected by the previous experiments.

Certainly the ultimate goal of all studies in ^{229m}Th is a direct optical control of the isomeric nuclear transition via laser excitation. However, this implies an improved knowledge of the transition wavelength by at least an order of magnitude.

In view of the promising properties of ^{229m}Th , it is not surprising that this nuclear transition is studied by many groups world-wide. Different projects are presently pursued, basically following two main experimental concepts, where the first one builds upon doping host crystals with ^{229}Th and subsequent photo-excitation either directly or via electronic bridge processes. The other concept draws on investigating thorium recoil ions from ^{233}U α decay, exploiting the 2% decay branch to the isomeric state and targeting an excitation of the isomeric state in an ion trap (e.g. linear Paul trap).

At the Lawrence Livermore National Laboratory (USA), where the revised transition energy of ^{229m}Th has been determined, further experiments are ongoing aiming at a measurement of the so far only theoretically estimated isomeric half life of ^{229m}Th by searching for conversion electrons or photons from conversion decays [13]. Via a population of ^{229m}Th from the α decay of ^{233}U the recoil ions are caught and brought between a detector setup of MCP and UV photomultiplier. A

determination of the so far unknown half life of ^{229m}Th would result in an improved value of the natural line width of the ground-state transition from the isomeric excited state.

The project pursued at the University of California (Los Angeles, USA) draws on the high photon flux of the Berkeley Advanced Light Source (ALS), where based on a 1.9 GeV electron synchrotron 10^{16} ph/sec are available at a bandwidth of 0.175 eV. In Ref. [14], a new approach for a direct identification of the excitation energy of the low-lying isomer in ^{229}Th was proposed. ^{229}Th nuclei, implanted in a host crystal, should be photo-excited into the isomeric first excited state in the ALS, with subsequent investigation of the induced fluorescence. In order to determine the transition frequency, the photon energy should be scanned in steps of 0.5 eV, thus an envisaged accuracy of the transition wave length of about 0.1 nm is targeted.

At Georgia Tech University (USA), the development of the laser cooling of highly charged Th^{3+} is in the research focus. For the long-lived ^{232}Th laser cooling could already be demonstrated [15] and recently a proposal for a virtual clock transition composed of stretched states within the $5F_{5/2}$ electronic ground level of both nuclear ground and isomeric manifolds was proposed and shown to offer unprecedented systematic shift suppression, allowing for clock performance with a total fractional inaccuracy approaching 10^{-19} [16].

At the Physikalisch-Technische Bundesanstalt in Braunschweig (Germany), after a basic study to outline the potential of $^{229m}\text{Th}^{(3+)}$ qualifying as an ultra-stable nuclear frequency reference [9], now a proposal is pursued towards a novel experimental scheme to excite the nuclear transition $^{229g}\text{Th} - ^{229m}\text{Th}$ in Th^+ ions for a determination of the transition frequency. Based on theoretical calculations [17], the recently proposed scheme [18] employs a bridge process, driven by two incoming laser photons, whose summed frequency resonantly corresponds to the transition frequency.

Also recently a new project started at the TU Vienna (Austria) [19]. Here ^{229}Th ions will be implanted into a UV-transparent crystal (e.g. CaF_2 , LiCaAF_6), finally aiming at the realization of an optical, solid-state-based nuclear clock. In this concept, the complex vacuum systems of present atomic clocks could be replaced by a single crystal, doped with ^{229}Th atoms at room temperature. A collaborative project is pursued at the IGISOL facility in Jyväskylä (Finland) together with the University of Mainz (Germany), aiming at the identification of the 7.6 eV isomer via a measurement of its hyperfine structure [20]. This project is closest to our experimental approach, since here also a ^{233}U recoil buffer-gas cell is applied [21] (see also Sect. 2.1. Preparatory work has been performed using Resonance Ionization Spectroscopy (RIS) to measure isotope shifts of $^{228,229,230}\text{Th}$ and a template of the ground-state hyperfine structure of ^{229}Th has been established for a 261.24 nm UV transition.

Moreover, the outlined extensive experimental quest for the low-energy ^{229}Th isomer has also been assisted and guided by comprehensive theoretical efforts both within atomic physics and nuclear theory, see e.g. Ref. [10, 19, 22, 23, 24, 25, 26, 27].

2. Experimental approach

The experimental approach pursued by our group towards an unambiguous and largely from potential background contributions separated identification of the UV deexcitation of the isomeric excited state in ^{229}Th is based on a spatial decoupling of population and deexcitation of the low-

lying first excited state. This approach is enabled by the availability of a highly efficient buffer-gas stopping cell that has been developed in Garching. Here the population of the isomeric first excited state of ^{229}Th can be achieved via α decay of ^{233}U . In order to achieve this, an experimental setup has been realized, which has been characterized in first preparatory measurements and is being continuously improved. This provides an excellent starting point for a targeted search for the isomeric ground-state transition in ^{229}Th and the subsequent development of an optical excitation scheme. In the following sections, the various steps of the experimental approach will be reviewed.

2.1 Stopping and extraction via a buffer-gas cell

Fig. 2 shows the setup of the 'MLL IonCatcher', which is operated at the Maier-Leibnitz Laboratory in Garching [28]. It consists of a system of two vacuum chambers, strictly built according to UHV standards. The first chamber, the buffer-gas stopping cell, serves to stop energetic ions in an atmosphere of ultra-pure helium gas (pressure ca. 25-50 mbar), before guiding them via radio-frequency and DC fields towards a nozzle exit, where they are dragged out of the chamber via a supersonic gas jet into the subsequent extraction chamber. Hereby, the DC guiding field in the gas cell provides a controlled acceleration of the stopped ions towards the nozzle. In order to guide also ions from regions away from the gas-cell axis towards the nozzle throat, a radiofrequency funnel is applied. This is a system of 50 ring electrodes, with diameters that conically continuously reduce towards the nozzle. The electrodes are electrically isolated with respect to each other and are connected to an RF phase alternating by 180° from one electrode to the next. In addition to the RF amplitude, they are provided with a DC gradient in the direction of the nozzle. This results in an accelerating force onto the ions towards the nozzle, while the radiofrequency field exerts a repelling force of the electrodes onto the ions. In total this leads to a funnel-like guidance of all ions to the nozzle exit, where the gas flow of the supersonic jet that forms in the nozzle drags the ions off the field lines, transporting them into the extraction chamber that houses a radiofrequency quadrupole (RFQ) acting as ion guide and phase-space cooler. In order to minimize ion losses from recombination or molecule formation inside the gas cell, both chambers have been built strictly according to UHV standards, i.e. avoiding any organic materials inside the cell by using only stainless steel and ceramic components, providing baking capability (up to 180°) and, after evacuation to $\leq 10^{-11}$ mbar, are operated with catalytically purified (gas purity ca. 1 ppb) ultra-clean He 6.0, fed in via electropolished tubes and further purified by a cryotrap in front of the cell entrance.

The described setup of the buffer-gas cell with its RF- and DC extraction electrode systems is shown Fig. 2 together with the subsequent extraction chamber and its radiofrequency quadrupole. This RFQ serves to transport the ions behind the gas cell, to separate them from the carrier gas behind the extraction nozzle and particularly it acts as phase-space cooler for the ions behind the gas cell.

High-resolution mass measurements behind the extraction RFQ have proven quantitative removal of water and oxygen contaminants, a crucial prerequisite for an efficient ion extraction. This buffer gas cell ('MLL-IonCatcher', [28]) is an optimized second generation of the buffer gas cell built by the LMU group for the SHIPTRAP project at GSI [29]. The SHIPTRAP gas cell is routinely very successfully used for measurements of high-precision nuclear mass measurements of heavy transactinide isotopes at the Penning trap system SHIPTRAP. From the experience at SHIP-

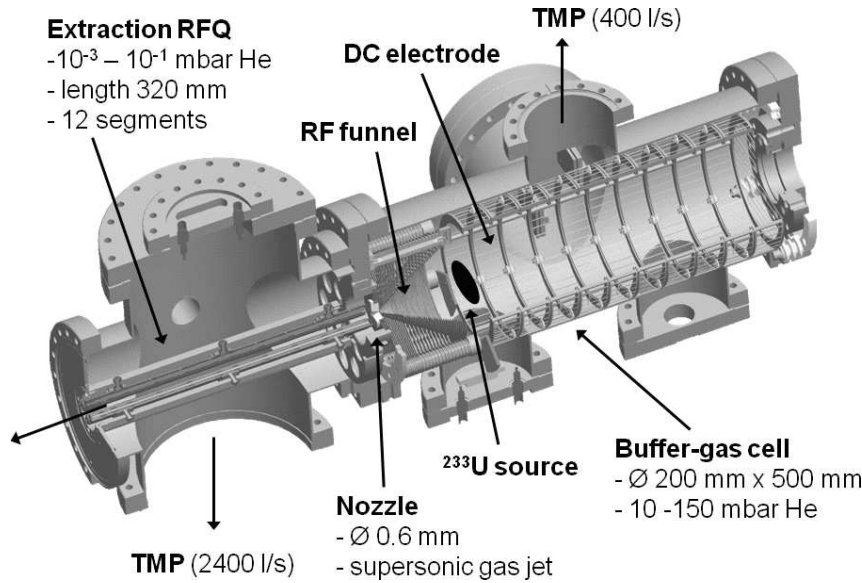


Figure 2. Schematical setup of the buffer-gas stopping cell at the Garching Maier-Leibnitz-Laboratory (MLL-IonCatcher).

TRAP we know that the dominant fraction of ions leave the gas cell in a doubly-charged state due to the low probability of charge-exchange reactions in the ultra-pure environment.

This device enables us to choose a novel approach in the investigation of ^{229m}Th , allowing for an efficient suppression of background contributions during the search for the UV fluorescence of the ground-state transition of ^{229m}Th .

2.1.1 Population and Extraction of ^{229m}Th using the gas cell

While presently a direct population of the thorium isomer via laser excitation still fails due to the extremely narrow line width of the transition together with an rather unprecise knowledge of the transition energy, instead the α decay of ^{233}U to ^{229}Th can be used for a population of the isomer. This is provided by a decay branch with an intensity of about 2%, leading from ^{233}U to the first excited state of ^{229}Th .

We placed a radioactive ^{233}U source (evaporated onto a steel backing) inside the above described 'MLL-IonCatcher' buffer-gas stopping cell (presently using an effective source activity of 5 kBq), such that the ^{229m}Th α recoil nuclei produced during the α decay will be stopped in about 40 mbar helium and then will be guided by the RF and DC fields as described before to the nozzle exit of the gas cell. Here they are transferred by the gas flow into the vacuum regime of the subsequent RFQ phase-space cooler and ion transport channel. The extraction from the gas cell can be performed within 1-2 ms.

This experimental arrangement assures that all background processes like conversion or prompt excitations happen inside the gas cell, while only α recoil nuclei will be extracted, thus eliminating the contamination by prompt background processes.

From the decay chain of ^{233}U it turns out that besides ^{229m}Th also other short-lived α recoil nuclei can be expected behind the gas cell (^{221}Fr , ^{217}At , ^{213}Po). For the identification of extracted α recoil nuclei from the gas cell and to demonstrate the feasibility of collecting the recoil ions after

the extraction RFQ, in a first exploratory setup a steel needle tip set on an appropriate attractive potential to capture the extracted (positive) ions was mounted behind the RFQ, while a silicon particle detector was positioned sideways without direct sight to the RFQ exit. The resulting α energy spectrum is shown in Fig. 3.

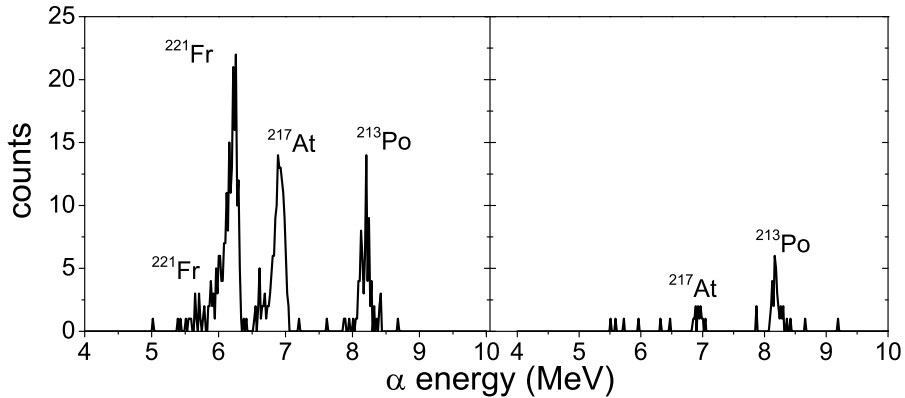


Figure 3. α -energy spectrum of daughter nuclei from the decay of ^{233}U after extraction from the gas cell and collection on a needle tip (left panel). The right panel shows a reference measurement (same measuring time), where the extracted ions were collected onto a plate located out of sight from the silicon detector. In this case the direct α -decay line from ^{221}Fr disappears and only and only a weak component from ^{213}Po remains, originating from the decay of ^{217}At recoil ions, implanted during the decay of ^{221}Fr at sites visible from the detector position.

We find in the left panel the α spectrum of ^{233}U daughter nuclei. As a proof that it indeed originates from α decays on the needle tip and not from otherwise implanted recoil nuclei, a reference measurement was performed, where the collection potential was chosen such that ions were accumulated on a plate that in the previous case served as electrostatic reflector to achieve a soft collection of ions on the needle tip. Now the silicon detector was mounted without direct sight to the collection surface. This leads to the spectrum shown in the right panel, where the previously dominant line from ^{221}Fr has disappeared and only a weak component from ^{213}Po remains, originating from the decay of ^{217}At ions, implanted during the decay of ^{221}Fr at sites visible from the detector position.

This proves in principle the feasibility of the described production scheme for $^{229\text{m}}\text{Th}$, while still calling for an optimization of the collection efficiency and a purification of the extracted ions from decay products other than ^{229}Th .

In a first step the extraction efficiency out of the gas cell was determined using a ^{223}Ra α recoil source. From the identification of the α decay of the ^{215}Po decay products, an extraction efficiency of 48% could be determined for this ion species [30]. However, we do not claim this efficiency also to be valid for the extraction of ^{229}Th in view of experimental findings at the IGISOL facility in Jyväskylä [21]. There a rather high reduction factor of 10 was observed between the efficiency measured for $^{221}\text{Fr}^+$ and $^{229}\text{Th}^+$, which was assigned to reactive impurities in the buffer gas like oxygen or water. Since cleanliness in the gas cell as well as for the used He gas was a design criterion from the start and could already be demonstrated in sensitive mass spectrometry, exceeding the provisions included in the IGISOL setup in several aspects (efficient RF funnel structure, baking

capability to $\sim 180^\circ$, electropolished tubing with VCR fittings, catalytic purification of highest-grade He 6.0), we are confident that it is fair to assume a reduced loss factor of 5 instead 10 for the MLL-IonCatcher, thus ending with about 10% extraction of ^{229}Th . However, as shown later, even without this factor of 2 higher extraction efficiency, enough detectable photon rate and signal contrast could be achieved. Moreover, we assume 70% population of the 2^+ charge state, derived from our experience at the SHIPTRAP gas cell, where Penning-trap mass measurements routinely use 2^+ ions from the gas cell. Thus our best estimate for the expected extraction efficiency of $^{229}\text{Th}^{2+}$ is 7%.

While we are presently limited by the total ^{233}U source activity of 15 kBq, corresponding to a usable Th recoil intensity of 5.0 kBq and finally ca. 7 extracted ^{229m}Th isomers per second, we have in the meanwhile obtained a license to handle a total source activity of up to 260 kBq, thus opening the perspective to further increase the Th flux by a factor of about 16 (with the final limiting factor being the maximum diameter of about 90 mm for the ^{233}U source inside the gas cell). Producing such a large-area source via electro-plating requires great care to achieve good surface homogeneity in view of the thin ^{233}U layer to be realized (ca. 13 nm). Moreover, one has to avoid any chemical contaminations from the source production process on the source surface that could be transferred as gas impurities into the ultra-pure He buffer gas via surface sputtering during the α decay process. Here one has to take into account already the unavoidable oxide contamination introduced by using uranium oxide instead of the more favourable, however highly oxidizing metallic uranium.

2.2 RF mass filter for exclusive extraction of ^{229}Th α recoil nuclei

From the α energy spectrum (Fig. 3) measured behind the gas cell it is obvious, that not only the direct α daughter nucleus ^{229}Th , but also the further decay products ^{225}Ra and ^{221}Fr can be extracted from the gas cell, potentially also acting as sources of subsequent UV fluorescence. Only with a full control over the recoil ions, as realized in our experimental approach of the ion transport through an RF ion guide to the detection section, an additional selection stage can be implemented, able to guarantee the requested unambiguity of the investigated ion species. In order to achieve this goal, the experimental setup has been extended by a quadrupole mass filter (QMS) behind the extraction RFQ. A first version that already achieved the required mass resolution of $\Delta m \sim 1$ (however at the expense of transmission efficiency) was recently replaced by a new device that was constructed following a novel and optimized design developed by the Giessen group [31], where besides utmost mechanical precision (tolerance of rod distances: 10 μm) Brubaker lenses [32] have been added at the entrance and exit of the QMS in order to allow for an optimized transmission efficiency. Fig. 4 shows a sketch and a photograph of the QMS rod system (upper and middle part) and the complete device including the shielding tube and positioning posts (bottom part).

Hereby, a selective transport of Th ions with mass 229 will be enabled, with simultaneous efficient suppression of lower masses, particularly 225 (Ra) and 221 (Fr). Thus the achievable mass resolution of about $m/\Delta m \sim 160$ with the new QMS will be sufficient to guarantee exclusive extraction of ^{229}Th .

A prerequisite for this mass resolution is a precise adjustment of the two alternating RF phases at the QMS. An active (LabView-based) control system was implemented and successfully commissioned, where the actual RF amplitudes, read out via a precise (12-bit) PC-based oscilloscope emulation, were adjusted to each other by trimming a remotely tunable capacitor. Thus a relative

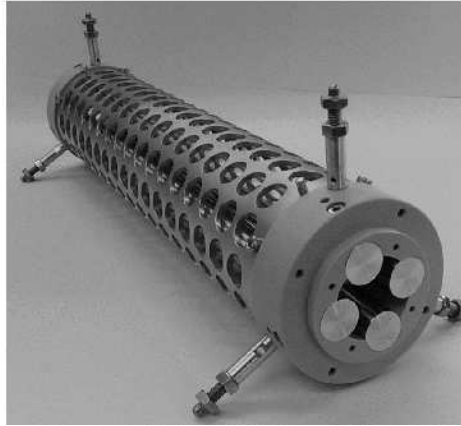
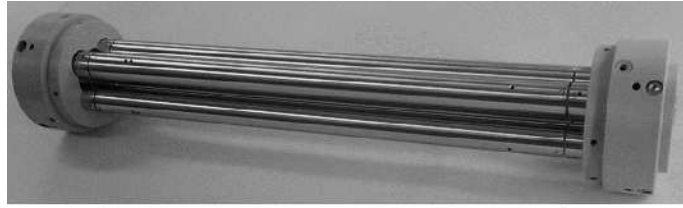
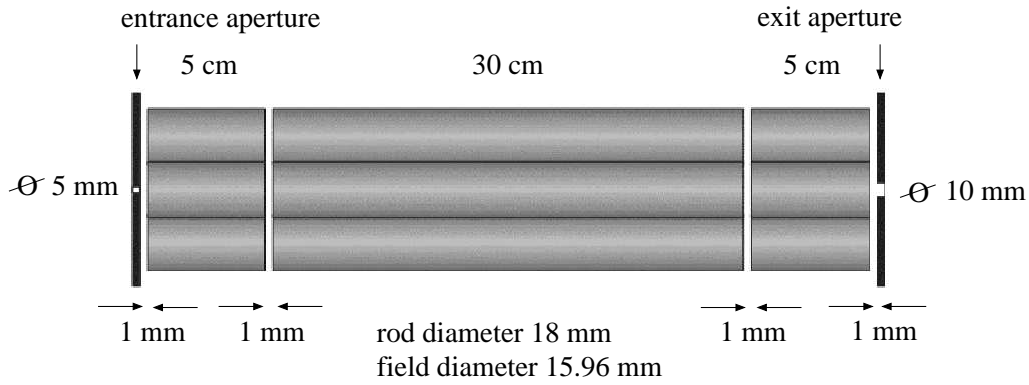


Figure 4. Quadrupole mass filter for an exclusive extraction of $^{229(m)}\text{Th}$ from the gas cell after α decay of a ^{233}U source. Upper and middle panel: sketch and photograph of the rod system (including Brubaker lenses at entrance and exit sides), bottom part: photograph of the full system including shielding tube and positioning posts.

accuracy of the two RF amplitudes of $\leq 1 \cdot 10^{-3}$ could be reached [33].

In order to characterize and optimize the mass filter, an alkali test ion source was integrated into the gas cell, able to provide $^{39,41}\text{K}$, $^{85,87}\text{Rb}$ and ^{133}Cs ions with sufficiently high rate for an optimization of the gas cell and QMS operational parameters. For these measurements an MCP detector for an individual registration of extracted ions is used instead of the Si detector used for the detection of α decays. Already with the predecessor version of the new QMS, a clear separation of the neighbouring mass peaks from $^{85,87}\text{Rb}$ could be achieved, while now the new device, will allow for a mass resolving power $m/\Delta m \sim 160$ (measured at 10% of the mass peak height) together with a transmission efficiency of about 80-90% as demonstrated in Ref. [31]. Thus the suppression of the accompanying α recoil nuclei ^{225}Ra and ^{221}Fr , which is mandatory for a selective extraction of $^{229(m)}\text{Th}$ from the gas cell, can safely be realized.

2.3 Setup of ion collection system

Ion trajectory simulations using the SIMION code package have been performed to design an optimized ion collection system behind the QMS exit by studying a wide variety of geometrical arrangements. During the simulations, the ions were followed over their full trajectory, starting from the ^{233}U source inside the gas cell, over the extraction RFQ and the quadrupole mass filter up to the final collection stage. Thus particularly the divergence of the ions exiting the QMS, which critically determines the achievable collection efficiency, could be realistically included in the optimization process. Design goals were (i) to achieve the highest possible ion collection efficiency and (ii) to realize the smallest possible collection surface in order to provide an almost point-like source for the targeted UV emission. Such a source will allow for a subsequent UV optics that minimizes the transmitted source image size onto the MCP detector in order to optimize the signal-to-background ratio.

Here the initial solution of attracting the ions via an electrical mirror onto a small (diameter $40\ \mu\text{m}$) steel needle tip positioned perpendicular to the extraction axis turned out to be inferior to another solution, where the ions are collected on a metallic surface (diameter $50\ \mu\text{m}$) directly facing the extraction axis. Moreover, in order to achieve a rather high ion collection, an attractive collection potential of $-500\ \text{V}$ needs to be applied at the collection surface. The simulated collection efficiency amounts to 40%, achieved by using a nozzle-like focusing electrode system behind the QMS exit as shown in Fig. 5 (left part). The middle part of Fig. 5 shows an enlarged view of the rectangle marked behind the nozzle exit, indicating the focusing and ion collection capabilities of the collection surface held at $-500\ \text{V}$.

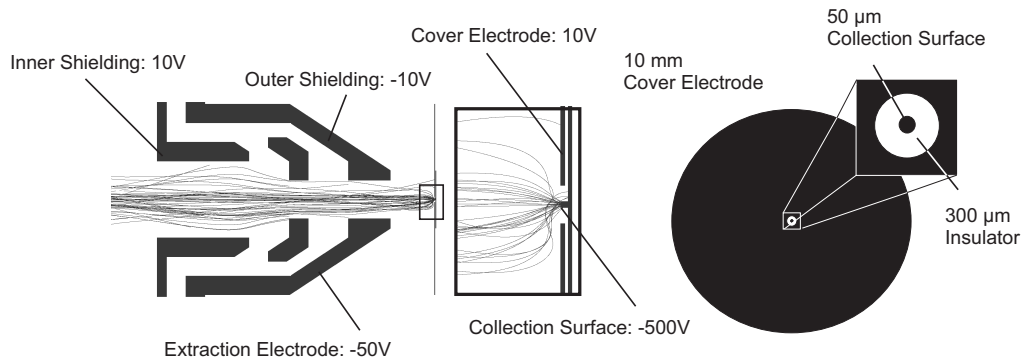


Figure 5. Schematical drawing of the nozzle-like electrode setup together with simulated ion trajectories (left) to focus ions entering from the QMS for efficient collection onto a small collection surface (right). In the middle part an enlarged view (corresponding to the region inside the marked rectangle) is displayed to highlight the focusing and collection properties.

The right part displays a front view of the collection surface ($50\ \mu\text{m}$ in the center, detailed view given in the inset), which is surrounded by an insulating rim (diameter $300\ \mu\text{m}$) and an outer cover electrode (diameter $10\ \text{mm}$). This structure has been manufactured by laser-drilling and etching from a polyimide laminate PCB, Cu-coated on both sides.

2.4 Provisions against quenching processes

When discussing the de-excitation of the excited isomeric ^{229m}Th state, we have to take into account the possibility of a non-radiative deexcitation, i.e. a quenching process originating from a surface interaction between the collected (excited) Th ions ('donor') and the collection surface ('acceptor') [22]. Several mechanisms of this energy transfer are usually described in the context of fluorescence chemistry. In our case the Förster resonance energy transfer (FRET) [34] will be the most important one. The FRET mechanism is based on a dipole-dipole interaction between the donor and the acceptor. Due to this interaction a virtual photon, which violates energy conservation, can be interchanged over distances of up to 10 nm. Within a QED description, the possibility of quenching is connected to the emission and absorption spectral overlap between donor and acceptor. In case that no such spectral overlap exists, no quenching can occur [35], meaning that in our experiment quenching can be ruled out in case the collection of the isomers takes place on a surface (of thickness larger than 10 nm) with no spectral absorption in the vacuum-UV region around 160 nm. This can be achieved by coating the collection surface, e.g., with MgF_2 , which is a standard material used for protective coatings of Al mirrors. Thus we propose an MgF_2 -coated metallic surface as ion collection electrode, where the thin dielectric layer will not affect the collection properties of the electrode operated at ~ 500 V, e.g., by surface charging effects [36] due to a small current in the dielectric material, large enough to a direct discharge.

In order to obtain a more quantitative assessment of radiationless deexcitation processes, we propose to measure the effect of quenching in a separate experiment, e.g. by using atomic species with UV transitions that are easier to access compared to ^{229}Th . This way the amount of quenching could be quantified and the above proposed method to prevent radiationless deexcitation could be tested.

2.5 Optimizing the UV focusing optics

Extensive simulations using an optical ray-tracing code, specifically developed for this purpose, were performed to benchmark different options for the UV optical system.

Optimization criteria were (i) a maximized photon collection efficiency and (ii) a small image magnification to achieve the best possible signal contrast ratio, the latter imposing strict requirements on the focal lengths of the optical elements, leading to contradictions with large numerical apertures favoured for (i) when using lens-based systems. Moreover, spherical aberrations also limit the performance of setups based on spherical optical elements. This naturally leads to consider setups based on parabolic mirrors, which are favourable compared to aspherical elements due to their larger acceptance and broader wavelength dynamics.

Possible arrangements to focus the UV radiation that have been comparatively studied are (A) a system of two convex lenses, (B) a system consisting of a parabolic mirror and a (spherical) convex lens, (C) a system consisting of a parabolic mirror and an aspherical lens and (D) a system of 2 parabolic mirrors (as schematically shown in Fig. 6), each representing the best what can be achieved within the considered type of optical arrangement.

It should be noted that the double-lens system in contrast to the mirror-based scenarios would still require the (highly inefficient) ion collection on a needle tip.

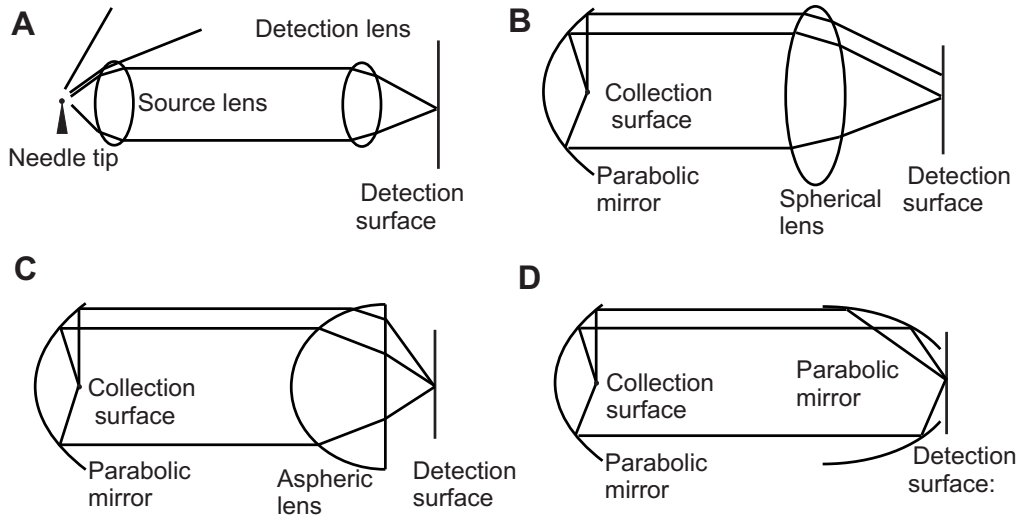


Figure 6. Schematical drawings of the four UV optical arrangements studied to focus the ^{229m}Th UV fluorescence onto an MCP detector.

Numerical results obtained for various properties of these optical systems are listed in Tab. 1. They represent the result of extensive calculations optimizing the optical system in the context of the full experimental setup in all operational parameters.

The image spot size is indicated here as the diameter of the photon distribution on the MCP detector given as FWHM value or at 10% of the peak maximum. From all scenarios studied, our favoured solution (scenario 'D' in Fig. 6) is an arrangement, where the collection surface is positioned in the focus of an annular parabolic mirror (dielectric coated aluminum mirror, outside diameter 40 mm, leaving a central hole of 12 mm diameter), which parallelizes the emitted UV light and transmits it onto a second parabolic mirror. This deep parabolic mirror is shaped via a central hole such that its retracted focal point lies in the plane of the MCP detector positioned directly behind the mirror. With an optical efficiency of 35.8% and typical reflectivities at 160 nm of 70% for each of the two mirrors, a total UV photon collection efficiency of 17.5% can be achieved. This arrangement allows for a small image size of ca. $70\ \mu\text{m}$ diameter, concentrating the UV flux onto only about 50 MCP pixels. Thus a very high signal contrast (see line (8) in Tab. 1 comparing to the MCP dark count rate) can be achieved. We also studied a scenario based on the first parabolic mirror and an aspheric lens replacing the second mirror, indicated as scenario 'C'. At first glance it appears as if this arrangement were even superior to the double-mirror setup discussed before (mostly owing to the difference between the assumed lens transmission of 85% compared to the mirror reflectivity of 70%, which, however, may be over-estimated for the actual thickness of 20 mm needed for the aspheric lens in our case). In fact, both scenarios 'C' and 'D' draw on the correction of the spherical aberration to reach their impressive performance. However, it should be emphasized that the values listed in Tab. 1 for setup 'C' only hold for the design wavelength of 163 nm, while significant degradation is found when deviating from this wavelength. As an example, considering a wavelength deviation of $\pm 10\ \text{nm}$, i.e. calculating setup 'C' for 153 nm and 173 nm, respectively, brings down the signal contrast from 398 (at 10% maximum height) to 154 (153 nm) or 176 (173 nm), ending up about a factor of 2 inferior to the double-mirror setup. Moreover,

Table 1. Properties of the four alternatively studied optical scenarios to focus the UV fluorescence radiation: (1) percentage of photons reaching the MCP, starting from source emission as 100%; (2) percentage of photons focused into image spot, taking all photons reaching the MCP as 100%; (3) percentage of photons focused into image spot, starting from source emission as 100%; (4) same as (3), but including lens transmission efficiencies (0.85) and mirror reflectivities (0.7); (5) absolute photon counting rate on MCP, starting from 2.24 isomer decays/sec. from collection surface (expected for case B, C and D), including MCP efficiency of 0.16 at 160 nm; (6) image spotsize obtained from numerical calculations, including source diameter and exact optical shapes; (7) image magnification as derived from source dimensions; (8) count rate divided by the expected image area; (9) image intensity divided by expected dark count rate of 0.05/s mm². The values listed for scenario C are given for a wavelength of 163 nm and degrade when deviating from this design value (in contrast to the performance of the double-mirror scenario D)

| | A: Double (spherical) lens | | B: Mirror / (spherical) lens | |
|---|----------------------------|---------|------------------------------|-------|
| | 10% | FWHM | 10% | FWHM |
| geometric acceptance [%] (1) | 2.4 | 2.4 | 40.5 | 40.5 |
| geom. collection efficiency [%] (2) | 40.4 | 10.1 | 79.0 | 25.5 |
| optical efficiency [%] (3) | 0.99 | 0.25 | 32.0 | 10.3 |
| photon collect. efficiency [%] (4) | 0.72 | 0.18 | 19.0 | 6.1 |
| counting rate [s ⁻¹] (5) | 0.0026 | 0.00064 | 0.068 | 0.022 |
| image spotsize [mm] (6) | 0.17 | 0.045 | 0.51 | 0.21 |
| effective image magnification (7) | 3.5 | 0.9 | 10.2 | 4.3 |
| image intensity [s ⁻¹ mm ⁻²] (8) | 0.11 | 0.40 | 0.34 | 0.61 |
| signal contrast (9) | 2.2 | 8.0 | 6.8 | 12.2 |
| | C: Mirror/aspherical lens | | D: Double mirror | |
| | 10% | FWHM | 10% | FWHM |
| geometric acceptance [%](1) | 41.4 | 41.4 | 41.3 | 41.3 |
| geom. collection efficiency [%](2) | 78.8 | 19.3 | 86.7 | 60.3 |
| optical efficiency [%](3) | 32.6 | 8.0 | 35.8 | 24.9 |
| photon collect. efficiency [%] (4) | 19.4 | 4.8 | 17.5 | 12.2 |
| counting rate [s ⁻¹] (5) | 0.069 | 0.017 | 0.063 | 0.044 |
| image spotsize [mm] (6) | 0.067 | 0.021 | 0.066 | 0.044 |
| effective image magnification (7) | 1.33 | 0.42 | 1.33 | 0.87 |
| image intensity [s ⁻¹ mm ⁻²] (8) | 19.9 | 50.7 | 18.1 | 29.3 |
| signal contrast (9) | 398 | 1015 | 362 | 586 |

one has to keep in mind that for an optimum performance of setup 'C' the focal position of the aspherical lens has to be defined with a precision of about 10 μm , which may turn out to be a time consuming effort in view of the about 2 mm shift of the focal length when varying the wavelength between, e.g., 153 nm and 173 nm, respectively. Assuming a step width of 50 μm , a maximum of 40 measurements will be required to search for the lens focus. Particularly when taking into account potential radiationless deexcitation processes and thus reduced detectable UV photon yield, the individual measurement time needed for each of these steps may rise up to 50 hours, rendering the search procedure a lengthy and maybe even prohibitive task. In view of the comparable count rates that can be achieved in either of the two cases (once the correct focal position of the aspher-

ical lens has been found), we consider both setups as viable options, where technical feasibility of the respective optical elements will finally decide on the realization, nevertheless with a clear preference for the double-mirror setup due to its less critical wavelength dependence as outlined above.

During the commissioning phase, a deuterium lamp (with a UV emission spectrum around 160 nm) will be positioned behind a $50\mu\text{m}$ pinhole in the collection chamber. This will allow for a characterization and optimization of the optical transmission and detection properties.

2.6 Detection of the $^{229\text{m}}\text{Th}$ UV fluorescence radiation

In order to detect the UV radiation originating from the deexcitation of the $^{229\text{m}}\text{Th}$ isomeric state captured on the collection surface described before, the above described UV optical system will be placed behind the collection surface, allowing to focus a large fraction of the 7.6 eV UV fluorescence light onto a CsI-coated, UV-sensitive multi-channel-plate detector (MCP: 75 mm diameter in Chevron geometry, channel diameter $10\mu\text{m}$). The electrons that are generated in the MCP will then be accelerated onto a phosphor screen, where they are converted into visible light, subsequently registered by a highly sensitive, low-noise CCD camera.

In contrast to a simpler detection scheme using a single photomultiplier, the pixel structure of the MCP (ca. 10^6 electron amplifier channels per cm^2) offers the opportunity to discard a majority of the dark count rate, provided an optimized focusing of the UV fluorescence. Typical dark count rates of MCP detectors of 0.05 counts/(sec. \cdot mm^2) result in a dark count rate of $5 \cdot 10^{-6}$ per pixel and second. When we therefore achieve to focus the image of the UV source onto 50 pixel of the MCP (corresponding to an image diameter of about $70\mu\text{m}$, which we expect from our simulations as diameter of the image spot), this corresponds to a background contribution to the signal strength in the image spot due to the MCP detector of $2.5 \cdot 10^{-4}$ /sec. This low dark count rate can by far not be reached by any low-noise single photomultiplier.

2.7 Improved determination of $^{229\text{m}}\text{Th}$ ground-state transition

The optical double-mirror setup introduced before has the additional advantage that it leaves ample space between the mirrors to install a filter system that can be used to determine the transition wavelength of $^{229\text{m}}\text{Th}$. Since the optical pathway will be parallel between the two mirrors, no effects from convergent or divergent optical paths through the mirrors have to be considered. Here we intend to apply a straightforward 'binary search' technique. As soon as the fluorescence signal from the $^{229\text{m}}\text{Th}$ decay has been unambiguously identified, the next project step will target to significantly improve the accuracy of the transition wavelength to better than 1 nm, corresponding to an improvement of about one order of magnitude compared to our present knowledge. This can be achieved by inserting special UV absorption filters with particularly sharp absorption edges into the direction of the focused fluorescence radiation, searching for a disappearance of the 7.6 eV signal. Fig. 7 visualizes this concept.

For this purpose, two specially coated VUV filter sets with absorption edges near 160 nm and 170 nm, respectively, with a width of the absorption edge of ca. 1 nm have already been purchased. More filters with fine-tuned absorption edges should be acquired depending on the coarse location of the transition energy determined with the existing filter sets. Moreover, using these filters, the position of the absorption edge can be varied by a variation of the entrance angle as indicated in

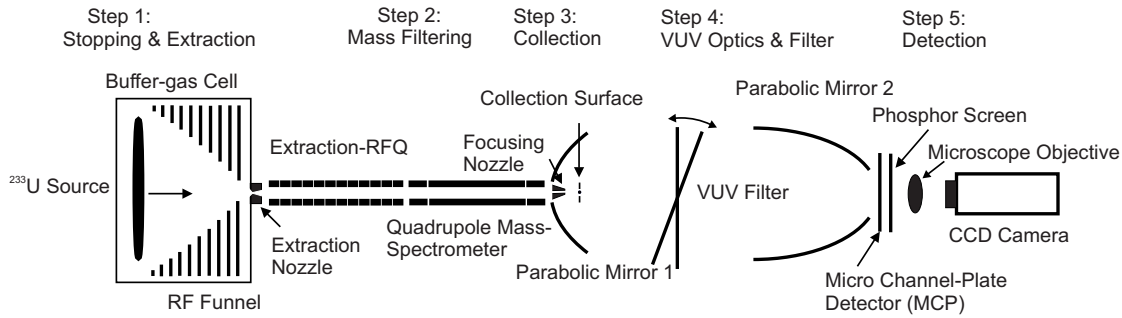


Figure 7. Experimental scheme for the identification of UV fluorescence from the deexcitation of the isomeric first excited state of ^{229m}Th .

Fig. 7. In order to achieve this the filter will be positioned on a remotely controlled rotary stage. With this rather straightforward method it will be possible to improve the present accuracy of the ground-state transition energy of the isomeric first excited state in ^{229}Th by about an order of magnitude, thus providing the prerequisites for the development of a dedicated laser system.

3. Concluding efficiency assessment and count rate estimate

Having quantitatively discussed all components of the experimental setup, we can finally present the full picture, outlining the various contributions to the final detection efficiency and specifying the expected count rate and signal contrast.

^{233}U α source: presently we are operating a ^{233}U source with an effective Th activity of 5.0 kBq. In the meanwhile, we have successfully applied for an increased handling license up to 260 kB total activity. In view of the 2π acceptance for recoil emission, taking into account the recoil stopping range of Th in U (ca. 10 nm), the actual chemical stoichiometry of the source material (U_3O_8) and considering the geometrical constraints inside the gas cell (limiting to a source diameter of 90 mm), a further increase of the effective (angle-integrated) Th flux by a factor of 16 up to 80 kBq can be achieved. Together with the 2% decay branch to the first excited isomeric state, presently 100 (future: 1600) ^{229m}Th ions per second enter the buffer gas stopping volume. It should be emphasized that the intended increase of the source area will not affect the extraction efficiency due to the guiding and focusing properties of the RF funnel.

Buffer-gas cell: As discussed in Sect. 2.1, we expect an extraction efficiency from the buffer-gas cell for $^{229m}\text{Th}^{2+}$ of 7%.

Mass filter: The QMS transport efficiency will amount to about 80%.

Ion collection: An ion collection efficiency of 40% is expected behind the QMS.

UV fluorescence focusing: according to the discussion in Sect. 2.5, about 17.5% of the emitted 7.6 eV photons will be focused by the double-mirror arrangement onto the detection device.

MCP detector: The detection efficiency at 160 nm for a CsI-coated and thus UV-sensitive MCP detector typically amounts to 16%.

Finally, this leads to total efficiency of $1.2 \cdot 10^{-5}$, corresponding to a detectable UV photon rate of 0.06/s for the present 5.0 kBq Th source, which can be increased to 0.96/s for a source

activity of 80 kBq as envisaged in the near future. In view of the focal spot size on the MCP of 70 μm diameter (area ca. 0.004 mm^2) and a typical MCP dark current of 0.05 counts/(s $\cdot\text{mm}^2$), even the present source strength would allow for a signal:background-ratio of 362:1, which could be increased further by a stronger source up to ca. 5800:1.

It should be stressed that with the present ^{233}U source and the double-mirror setup, already a superb signal contrast can be achieved, which is expected to be high enough to detect the $^{229\text{m}}\text{Th}$ de-excitation radiation even if significant non-radiative losses via bridge processes or conversion decays in the range of 90% occur. With the envisaged increased source activity by a factor of 16, our detection sensitivity could be increased to even as low as 1% of the expected deexcitation processes.

Thus we conclude that we present here an experimental concept that has been studied and designed quantitatively in all components, either via preparatory experimental work or by detailed simulations, ending in a scenario with high enough sensitivity to achieve a detection of the UV fluorescence from the low-lying isomeric first excited state of ^{229}Th even in case of unfavourable decay branchings and to target an improvement of the experimental accuracy of the ground-state transition.

Acknowledgments

We acknowledge fruitful discussions with T.W. Hänsch, T. Udem, D. Habs, E. Haettner, P. Hilz and J. Schreiber. This work was supported by the DFG Cluster of Excellence Munich-Centre for Advanced Photonics (MAP).

References

- [1] E. Peik and C. Tamm, *Nuclear laser spectroscopy of the 3.5 eV transition in Th-229*, *Eur. Phys. Lett.* **61** (2003) 181.
- [2] V.V. Flambaum, *Enhanced Effect of Temporal Variation of the Fine Structure Constant and the Strong Interaction in ^{229}Th* , *Phys. Rev. Lett.* **97** (2006) 092502.
- [3] J.C. Berengut et al., *Proposed Experimental Method to Determine α Sensitivity of Splitting between Ground and 7.6 eV Isomeric States in ^{229}Th* , *Phys. Rev. Lett.* **102** (2009) 210801.
- [4] L.A. Kroger and C.W. Reich, *Features of the low energy level scheme of ^{229}Th as observed in the α decay of ^{233}U* , *Nucl. Phys. A* **259** (1976) 29.
- [5] C.W. Reich and R.G. Helmer, *Energy separation of the doublet of intrinsic states at the ground state of ^{229}Th* , *Phys. Rev. Lett.* **64** (1990) 271.
- [6] R.G. Helmer and C.W. Reich, *An excited state of ^{229}Th at 3.5 eV*, *Phys. Rev. C* **49** (1994) 1845.
- [7] B.R. Beck et al., *Energy Splitting of the Ground-State Doublet in the Nucleus ^{229}Th* , *Phys. Rev. Lett.* **98** (2007) 142501.
- [8] B.R. Beck et al., *Improved Value for the Energy Splitting of the Ground-State Doublet in the Nucleus $^{229\text{m}}\text{Th}$* , *LLNL-PROC-415170* (2009), in proceedings of 12th Int. Conf. on Nucl. Reaction Mechanisms, 15 - 19 Jun. 2009, Varenna, Italy; eds. F. Cerutti and A. Ferrari, CERN-Proceedings-2010-001.

- [9] E. Peik et al., *Prospects for a Nuclear Optical Frequency Standard based on Thorium-229*, in proceedings of *7th Symposium on Frequency Standards and Metrology*, October, 5 – 11, 2008, Pacific Grove, CA/USA, (2009) 532-538, .
- [10] E. Litvinova et al., *Nuclear structure of lowest ^{229}Th states and time-dependent fundamental constants*, *Phys. Rev. C* **79** (2009) 064303.
- [11] V.V. Flambaum et al., *Coulomb energy contribution to the excitation energy in ^{229}Th and enhanced effect of α variation*, *Europhys. Lett.* **85** (2009) 50005.
- [12] V.V. Flambaum and R.B. Wiringa, *Enhanced effect of quark mass variation in $\text{Th}229$ and limits from Oklo data*, *Phys. Rev. C* **79** (2009) 034302.
- [13] E. Swanberg et al., *Searching for the Decay and Half Life of the 7.6 eV Excited State in the Thorium-229 Nucleus*, *Am. Phys. Soc.* **F1.002** (2011).
- [14] W.G. Rellergert et al., *Constraining the Evolution of the Fundamental Constants with a Solid-State Optical Frequency Reference Based on the $\text{Th}229$ Nucleus*, *Phys. Rev. Lett.* **104** (2010) 200802.
- [15] C.J. Campbell et al., *Multiply Charged Thorium Crystals for Nuclear Laser Spectroscopy*, *Phys. Rev. Lett.* **102** (2009) 233004.
- [16] C.J. Campbell et al., *Single-Ion Nuclear Clock for Metrology at the 19th Decimal Place*, *Phys. Rev. Lett.* **108** (2012) 120802.
- [17] S.G. Porsev and V.V. Flambaum, *Electronic bridge process in $\text{Th}229^+$* , *Phys. Rev. A* **81** (2010) 042516.
- [18] S.G. Porsev et al., *Excitation of the Isomeric ^{229m}Th Nuclear State via an Electronic Bridge Process in $^{229}\text{Th}^+$* , *Phys. Rev. Lett.* **105** (2010) 182501.
- [19] G.A. Kazakov et al., *Performance of a 229 Thorium solid-state nuclear clock*, *arXiv:1204.3268v2 [physics.atom-ph]*.
- [20] S. Raeder et al., *Resonance ionization spectroscopy of thorium isotopes - towards a laser spectroscopic identification of the low-lying 7.6 eV isomer of ^{229}Th* , *Jour. Phys.* **B 44** (2011) 165005.
- [21] V. Sonnenschein et al., *The search for the existence of ^{229m}Th at IGISOL*, *Eur. Phys. Jour. A* **48** (2012) 52.
- [22] E.V. Tkalya, A.N. Zherikhin and V.I. Zhudov, *Decay of the low-energy nuclear isomer $^{229}\text{Th}^m(3/2^+, 3.5 \pm 1.0 \text{ eV})$ in solids (dielectrics and metals): A new scheme of experimental research*, *Phys. Rev. C* **61** (2000) 064308.
- [23] E.V. Tkalya, *Properties of the optical transition in the ^{229}Th nucleus*, *Physics-USpekhi* **46** (2003) 315.
- [24] E.V. Tkalya, *Proposal for a Nuclear Gamma-Ray Laser of Optical Range*, *Phys. Rev. Lett.* **106** (2011) 162501.
- [25] F.F. Karpeshin et al., *Study of ^{229}Th through laser-induced resonance internal conversion* *Phys. Lett. B* **282** (1992) 267.
- [26] F.F. Karpeshin and M.B. Trzhaskovskaya, *Resonance Conversion as the Predominant Decay Mode of ^{229m}Th* *Hyp. Int.* **162** (2005) 125.
- [27] F.F. Karpeshin and M.B. Trzhaskovskaya, *Impact of the electron environment on the lifetime of the $^{229}\text{Th}^m$ low-lying isomer* *Phys. Rev. C* **76** (2007) 054313.

- [28] J.B. Neumayr, P.G. Thirolf et al., *Performance of the MLL-IonCatcher*, *Rev. Sci. Instr.* **77** (2006) 065109.
- [29] J.B. Neumayr et al., *The ion catcher device for SHIPTRAP*, *Nucl. Instr. Meth.* **B 244** (2006) 489
- [30] P.G. Thirolf et al., *Optical Access to the Lowest Nuclear Transition in ^{229m}Th* , *Annual Report of the Maier-Leibnitz Laboratory, Garching* (2007) 18.
- [31] E. Haettner, *A novel radio frequency quadrupole system for SHIPTRAP & New mass measurements of rp nuclides*, PhD thesis, Univ. Giessen (2011).
- [32] W.M. Brubaker, *An improved quadrupole mass analyser*, *Advances in mass spectrometry* **4** (1968) 293.
- [33] D. Kalb, *Entwicklung eines Regelsystems zum Präzisionsabgleich der RF-Amplituden eines Quadrupol-Massenspektrometers*, Bachelor Thesis, LMU Munich (2012).
- [34] Th. Förster, *Zwischenmolekulare Energiewanderung und Fluoreszenz*, *Ann. Physik* **437** (1948) 55.
- [35] R.P. Haugland et al., *Dependence of the kinetics of singlet-singlet energy transfer on spectral overlap*, *Proc. Nat. Acad. Sci.* **63** (1969) 23.
- [36] P.P. Budenstein et al., *Destructive Breakdown in Thin Films of SiO , MgF_2 , CaF_2 , CeF_3 , CeO_2 , and Teflon*, *Jour. Vac. Sci. Tech.* **6** (1969) 193.